2017

High-performance hybrid carbon nanotube fibers for wearable energy storage

Zan Lu
University of Wollongong

Yunfeng Chao
University of Wollongong, yc682@uowmail.edu.au

Yu Ge
University of Wollongong, yg711@uowmail.edu.au

Javad Foroughi
University of Wollongong, foroughi@uow.edu.au

Yong Zhao
University of Wollongong, yz705@uowmail.edu.au

See next page for additional authors

Publication Details

Lu, Z., Chao, Y., Ge, Y., Foroughi, J., Zhao, Y., Wang, C., Long, H. & Wallace, G. G. (2017). High-performance hybrid carbon nanotube fibers for wearable energy storage. Nanoscale, 9 (16), 5063-5071.

High-performance hybrid carbon nanotube fibers for wearable energy storage

Abstract
Wearable energy storage devices are of practical interest, but few have been commercially exploited. Production of electrodes with extended cycle life, as well as high energy and power densities, coupled with flexibility, remains a challenge. Herein, we have demonstrated the development of a high-performance hybrid carbon nanotube (CNT) fiber-based supercapacitor for the first time using conventional wet-spinning processes. Manganese dioxide (MnO2) nanoflakes were deposited onto the as-prepared CNT fibers by electrodeposition to form highly flexible nanocomposites fibers. As-prepared fibers were characterized by electron microscopy, electrical, mechanical, and electrochemical measurements. It was found that the specific capacitance was over 152 F g-1 (156 F cm-3), which is about 500% higher than the multi-walled carbon nanotube/MnO2 yarn-based supercapacitors. The measured energy density was 14.1 Wh kg-1 at a power density of 202 W kg-1. These values are 232% and 32% higher than the energy density and power density of MWNT/MnO2 yarn-based supercapacitor, respectively. It was found that the cyclic retention ability was more stable, revealing a 16% increase after 10000 cycles. Such substantial enhancements of key properties of the hybrid material can be associated with the synergy of CNT and MnO2 nanoparticles in the fiber structure. The use of wet-spun hybrid CNT for fiber-based supercapacitors has been demonstrated.

Disciplines
Engineering | Physical Sciences and Mathematics

Publication Details
Lu, Z., Chao, Y., Ge, Y., Foroughi, J., Zhao, Y., Wang, C., Long, H. & Wallace, G. G. (2017). High-performance hybrid carbon nanotube fibers for wearable energy storage. Nanoscale, 9 (16), 5063-5071.

Authors
Zan Lu, Yunfeng Chao, Yu Ge, Javad Foroughi, Yong Zhao, Caiyun Wang, Hairu Long, and Gordon G. Wallace

High-performance hybrid carbon nanotube fibers for wearable energy storage

Zan Lu[1, 2, 3], Yunfeng Chao[2], Yu Ge[2], Javad Foroughi[*2,4], Yong Zhao[2], Caiyun Wang[2], Hairu Long[1, 3], Gordon G. Wallace[*2]

1. College of Textiles, Donghua University, 2999 North Renmin Road, Shanghai, China.
2. Intelligent Polymer Research Institute, ARC Centre of Excellence for Electromaterials Science, University of Wollongong, NSW 2522, Australia.
3. Engineering Research Center of Technical Textile, Ministry of Education, Shanghai, China.
4. Illawarra Health and Medical Research Institute, University of Wollongong, NSW 2522, Australia.

Corresponding author: Foroughi@uow.edu.au, gwallace@uow.edu.au

[Insert Running title of <72 characters]

Abstract

Wearable energy storage devices are of practical interest, but few have been commercially exploited. Production of electrodes with extended cycle life, as well as high energy and power densities, coupled with flexibility, remains a challenge. Herein, we have demonstrated the development of a high-performance hybrid carbon nanotube (CNT) fiber-based supercapacitor for the first time using conventional wet-spinning processes. Manganese dioxide (MnO_2) nanoflakes were deposited onto the as-prepared CNT fibers by electrodeposition to form highly flexible nanocomposites fibers. As-prepared fibers were characterized by electron microscopy, electrical, mechanical, and electrochemical measurements. It was found that the specific capacitance was over 152 F/g (156 F/cm^3), which is about 500% higher than the multi-walled carbon nanotube/MnO_2 yarn-based supercapacitors. The measured energy density was 14.1 Wh/kg at a power density of 202 W/kg. These values are 232% and 32% higher than the energy density and power density of MWNT/MnO_2 yarn-based supercapacitor, respectively. It was found that the cyclic retention ability was more stable, revealing a 16% increase after 10,000 cycles. Such substantial enhancements of key properties of the hybrid material can be associated with the synergy of CNT and MnO_2 nanoparticles in the fiber structure. The use of wet-spun hybrid CNT for fiber-based supercapacitors has been demonstrated.

Introduction

Today we associate ‘wearable technologies’ with electronic devices like wrist bands for fitness and health monitoring. However, the fastest growth sector in the coming years is predicted to be smart garments where the electronics are incorporated into the fabrics. Recent developments in advanced materials are poised to create significant new opportunities for the

development of smart textiles. The growth projections for smart garments are based around seamless and invisible integration of the electronic functionality into the garment, but with aesthetic appeal and comfort continuing to be priorities. Strategies to achieve this objective do not yet exist and represent challenges for materials researchers to produce fibers and fabrics with the desired electronic functionality without compromising strength, comfort and aesthetic appeal. Similarly, the development of electronic textiles requires a re-think of the circuit design to optimise performance of these non-conventional electronic materials. Fiber-based supercapacitors (FSCs) can be readily integrated into textiles or garments to power a wire or cable type sensor or transistor, and to be an energy reservoir to store harvested energy from conversion systems including fuel and solar cells and thermoelectric or piezoelectric generators [1-6]. Studies of fiber-like electrode materials mainly focus on the development of novel materials that can be formed as a fiber or composited with other fibers/yarns like carbon fibers, cotton yarns and polymer fibers [7, 8] Another point of interest is the improvement of fiber structure by using techniques to obtain high-performance fibers with larger specific surface area, that could be integrated into traditional textiles structures [9, 10].

CNT materials already show promising performance for a myriad of applications including supercapacitors, actuators, and lightweight electromagnetic shields [11-14]. Carbon nanotubes are widely used electrode materials that possess extraordinary physical and chemical properties, and assemblies of CNTs in fiber format have been shown to be a viable platform to take these properties from the nanoworld to microscopic structures [15, 16]. CNTs can be grown as a forest using a variety of methods, from which they can be drawn off and twisted into a CNT yarn (solid-state) for fabrication into fibers, yarns and fabric structures. While the potential of CNTs is impressive, they are limited for practical applications due to slow production rates, high costs

and limited functionality. Therefore, approaches that improve the formation of hybrid structures and expand on wet-spinning methods are important. By means of solid-state and wet-spinning approaches, continuous and large-scale CNT fibers/yarns have been obtained to be applied in the field of energy storage. Carbon based electrodes materials have been shown to be highly stable with less reduction in capacitance after an extensive number of cycles compared to other electrode materials [17, 18]. However carbon based supercapacitors still show limited capacitances because their active material has been based on bare carbon, hence completely dependant on electrochemical double layer capacitance. Combining carbon based materials with pseudocapacitance materials, such as metal oxides or conducting polymers, can significantly improve capacitance but these suffer from poor energy density, limited stability with increasing cycle numbers [19, 20]. CNT fibers have been shown to be promising candidates for electrodes in a supercapacitor or lithium battery when composited with active materials such as MnO_2, polyaniline (PANI), polypyrrole (PPy), $LiMn_2O_4$, and $LiFeO_4$ [21-26]. Consequently there is still challenging for the development of high-performance hybrid wet-spun single-walled carbon nanotube/ manganese oxide fibers based supercapacitor [23, 27, 28].

In this study, we developed the use of hybrid carbon nanotube fibers to be used as highly performing wearable supercapacitors. High-performance hybrid wet-spun liquid crystal CNT fiber-based supercapacitors have been prepared using a wet-spinning process followed by electrodeposition of MnO_2 onto the as-prepared CNT fibers. Manganese dioxide was introduced into the fibers with a view to improving electrochemical properties. The resulting supercapacitor is highly flexible and possesses superior electrochemical properties in terms of high energy and power densities, dramatic cyclic stability and specific capacitance.

Experimental Details

Long, conductive fibers were wet-spun from liquid crystalline dispersions of single-walled carbon nanotubes. The liquid crystalline state of the dispersion greatly enhances the spinnability of the fibers, as well as the mechanical properties. Preparation of liquid crystal CNT spinning solution, fibers spinning and their characterization were carried out as previously reported [29]. Single-walled carbon nanotubes (SWNTs) were used as purchased (Nano-lab, USA). 35.7 mg SWNTs and 1 ml chlorosulfonic acid (CSA) (Sigma Aldrich) were mixed by using Thinky ARE-250 mixer for 20 min, and then the spinning dope was transferred into a 5 ml glass syringe. This process should be cautious and protected with safety suit regarding to the risk and danger causing by CSA. The syringe needle was 22G, and the pump extruded the dope into an acetone bath at a fixed rate of 25 ml/h and the rotating speed was 20 r/min. The prepared wet-spun liquid crystal CNT fibers were then washed with distilled water thrice and dried in an oven at 120 ℃. The structures were characterized by scanning electron microscopy (SEM, JEOL JSM-7500 operated at 5 kV), wet-state cross-section morphologies were also observed by SEM (JEOL JSM-6490 LV), transmission electron microscopy (TEM, JEOL JEM-2010 operated at 200 kV), Raman spectra (Jobin Yvon HR800, 632.8 nm diode laser), and X-ray photoelectron spectroscopy (XPS, PHOIBOS 100/150 with hemispherical energy analyzer).

Preparation of MnO_2 deposited CNT fibers and electrochemical performance measurement were as follows. All the fibers used for depositing were cut from the same long length of CNT fiber to a length of 2 cm. Each piece of fiber was stuck to a stainless steel wire using silver paste and then immersed in the electrochemical electrolyte for several minutes to ensure the fiber was fully saturated. The MnO_2 nanoplates were electrochemically deposited on the CNT fibers in an electrolyte of 0.02 M $MnSO_4 \cdot H_2O$ and 0.2 M Na_2SO_4 (Sigma Aldrich) at a potential of 1.3 V

with a three-electrode system (eDAQ, Australia), using Ag/AgCl as the reference electrode and Pt mesh as the counter electrode. After electrodeposition, the as-prepared fibers were washed with ethanol and distilled water several times and dried in an oven at 70 °C. Cyclic voltammetry (CV) of the fibers was scanned in 1 M Na_2SO_4 solution (CHI 604D, USA) at room temperature. In addition, electrochemical impedance spectra (EIS, Gamry EIS 3000 system) were obtained in the frequency range of 100 kHz to 0.01 Hz with an AC perturbation of 10 mV at open circuit potential, and galvanostatic charge/discharge tests were performed using a battery test system (Neware electronic Co.) from 0 to 1 V.

Fabrication of the solid-state FSC was achieved as follows. Due to the reaction between MnO_2 and acid, we use LiCl/PVA electrolyte rather than H_3PO_4/PVA or H_2SO_4/PVA electrolyte. PVA-LiCl gel electrolyte was prepared as described previously [30] by mixing 3 g PVA (Sigma Aldrich, Mwt 124-186 k) with 6 g LiCl (Sigma Aldrich) in 30 mL Milli-Q water and stirring at 90 °C until the solution became transparent. Two prepared carbon nanotube fiber (CNFs) or MnO_2-CNT fiber (MCFs) were coated with solid electrolyte several times and dried for 1 h each time. Then, two PVA-LiCl coated fibers were mounted in parallel on a flexible PET membrane, each end of the electrode was fixed by silver paste and extended with a stainless steel wire (100 µm, diameter) and finally coated with PVA- LiCl along the paralleled part to form a solid-state FSC.

Results and Discussion

The fabrication process to produce wet-spun liquid crystalline CNT fibers is shown schematically in Figure 1a. The single-walled nanotubes used in this study were commercially available and typical of products prepared by the chemical vapor deposition (CVD) method, with an average diameter of 1.5 nm and lengths of 1-5 µm. As described previously Chlorosulfonic

acid was used to prepare the single-walled or low-walled carbon nanotubes dispersion, a higher number of walls will lower the specific strength of fiber, which has been confirmed by us that the MWCNT wet-spun fibers are too brittle to be further applied [29]. As expected, the mixed dispersion went from an isotropic phase to a biphasic system and then to a single liquid-crystalline phase [31]. The prepared spinning dope was extruded into an acetone coagulation bath with a distance of 5 cm from the center of the bath container.

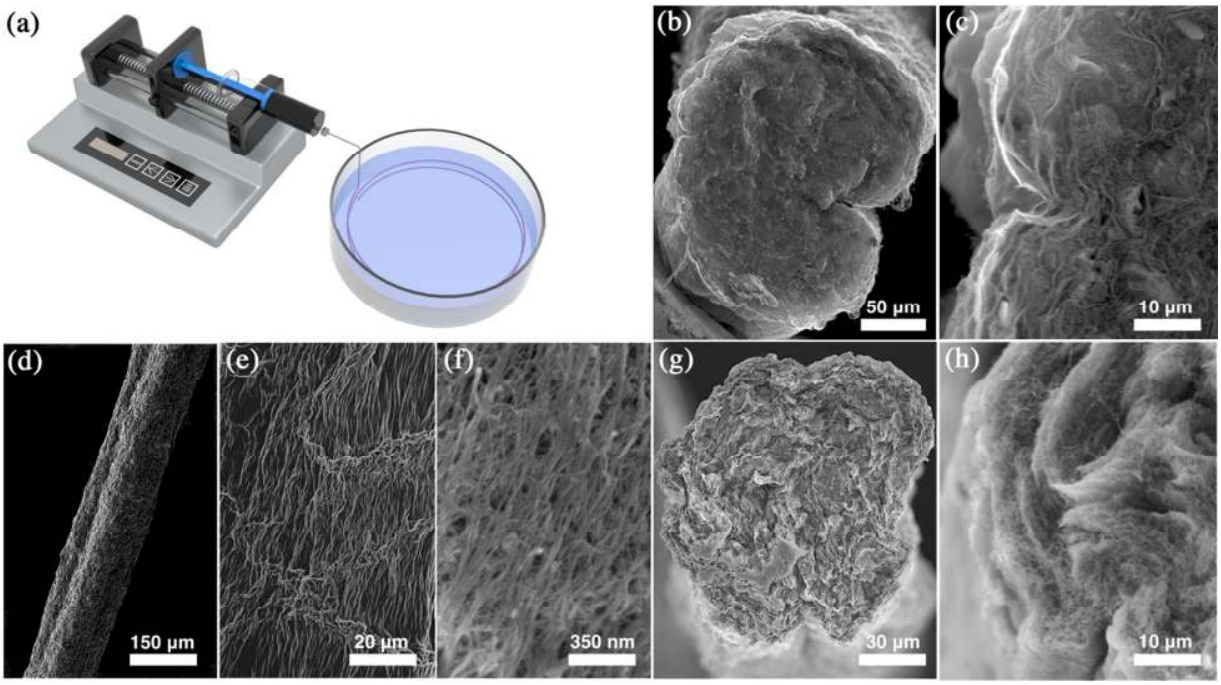

Figure 1. (a) Schematics of the preparation procedures for the wet-spun carbon nanotube fibers. (b) SEM images of a cross-section of wet-spun CNT fiber (wet-state) at low, and (c) higher magnification. (d) The surface morphology of as-prepared CNT fiber at (e) low and (f) higher magnification. (g) Cross-section of wet-spun CNT fiber (dry-state) at low and (h) higher magnification.

SEM micrographs of the as-spun pristine CNT fibers are shown in Figure 1 (b-h). SEM images of the cross-section of CNT fiber (wet) shows a porous structure (Figure 1c), in which

the pore size has a decreasing distribution from surface to inner fiber. We've also tried to freeze dry the wet fiber and observed the pores can be achieved at several microns in Figure S1. This morphology shrunk to form the wrinkled CNT layer-by-layer structure after drying in oven (Figure 1g-h, higher resolution of this structure can be found in the supporting information Figure S1). As can be seen from the surface morphology, nanotubes were uniform and predominantly oriented to the fiber axis (Figure 1d-f). The bundles of SWNTs and the inner nano-network structures can also be seen from the dried fiber surface at higher magnification (Figure 1f).

The diameter of the as-prepared CNT fiber as determined by the gauge of the spinneret, feed rate and drawing rate was 160 μm. The diameter of the CNT fiber obtained can be controlled to be as low as 50 μm [29]. To acquire the optimal performance of fiber, acetone was chosen as the coagulant because it dissolves CSA without reacting (unlike water, which forms hydrochloric acid (HCl) gas and sulfuric acid), which can damage the fiber structure. Because of its high volatility, acetone rapidly evaporates from the fiber once the fiber is removed from the bath and the residual acid will be removed by the following washing procedure. Comparing to the other coagulants (acetonitrile, chloroform, N, N-dimethylacetamide (DMA), deionized water, dimethyl sulfoxide (DMSO), ethanol, and hexanes), acetone bath is able to form highly conductive, strong, and uniform wires with minimal residual solvent, which has been studied by others recently [32]. The mechanical properties of as-spun CNT fibers achieved ultimate tensile strength, elastic modulus and elongation at break of 225 MPa, 23 GPa and 2% respectively. (See Figure S2 supporting information). While the tensile strength of the as-prepared CNT fiber was 246% higher that the previously reported wet-spun MWNT fiber [33], and 120% greater than the SWNT fiber by spinning from the fuming sulfuric acid as the solvent [34], the elastic modulus of

as-prepared fiber was quite low compared to pristine CNT fiber due to the porous nature of the wet-spun fiber. The electrical conductivity of the as-prepared CNT fibers was measured under laboratory conditions using an in-house linear four-point probe (see supporting information). The average electrical conductivity of the wet-spun CNT fibers was 450 ± 15 S/cm. It was found that the electrical conductivity of as-prepared CNT fiber was 50% and 114% higher than previously reported MWNT yarn or wet-spun CNT fiber, respectively.[35, 36]. The higher electrical conductivity of as-prepared CNT fiber suggests a lower contact resistivity between nanotube bundles; due to the highly aligned bundles of CNTs that were uniform and predominantly oriented to the fiber axis (Figure 1e-f). This phenomenon could imply an effective electron pathway for longitudinal current collecting.

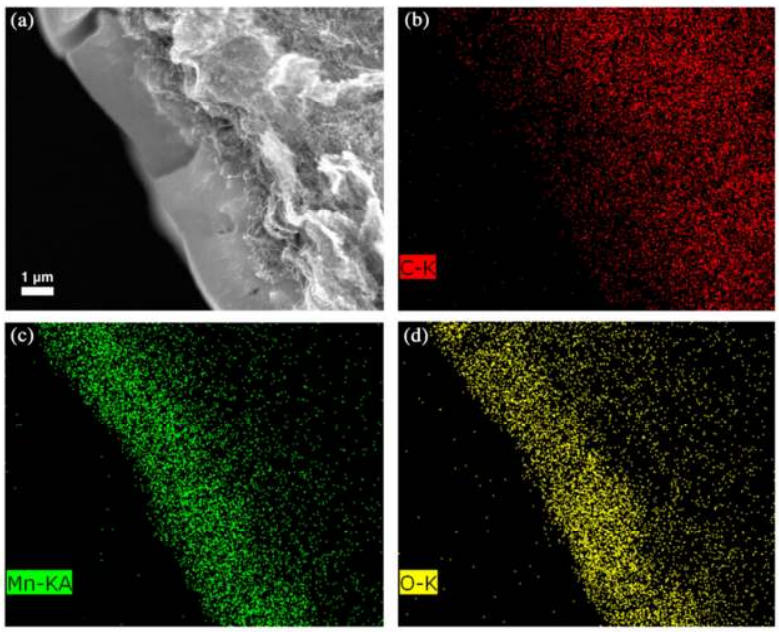

Figure 2. Elemental mapping analysis performed on: (a) the hybrid CNT/MnO_2 fiber cross-section area, (b) the location of carbon (C red dots), (c) manganese (Mn green dots) and (d) oxygen (O yellow dots) hybrid CNT/MnO_2 EDS image of a MnO_2 deposited CNT fiber.

With the merits of high conductivity, nano-network structure and superior mechanical properties, wet-spun CNT fibers show promise as excellent candidates for current collectors, active material carriers and active charge storage electrodes. Meanwhile, manganese dioxide is a promising pseudocapacitive material, because of its high theoretical capacitance, low cost, and environmental friendliness, to enhance dramatically its energy storage capacity [37]. MnO_2 was deposited on as-prepared wet-spun CNT fiber to make a hybrid CNT/MnO_2 fiber supercapacitor. MnO_2 can be effectively trapped in the pores during deposition due to the porosity inside wet-spun CNT fibers, resulting in formation of a well-blended zone that consists of nanostructured MnO_2 and aligned CNT bundles (Figure 2). As can be seen from elemental mapping analysis for C, O, and Mn atoms (Figure 2 a-d), the hybrid wet-spun CNT/MnO_2 fiber has a highly porous structure. This porosity is well distinguished by dominant Mn atoms detected from the fiber surface right to the core, after electrodeposition of MnO_2 (the location of Mn (red dots) in Figure 2c). The hybrid nanoscopic structure was confirmed through the overlapped C, O, Mn mapping images (Figure 2). In addition, the SEM images (Figure 3a, b, c) of MnO_2-CNT fiber (MCF) clearly shows that the flower-like MnO_2 nanostructures consist of a stack of nanoflakes with increased porosity of fiber; which can lead to the rapid transportation of electrons and ions when the fibers are assembled into supercapacitors. In addition, the transmission electron microscopy (TEM) image of Figure 3d indicates that the CNTs are overlaid with numerous MnO_2 nanoflakes. These pseudocapacitive nanoflakes play a crucial role in enhancing the energy storage performances of wet-spun CNT supercapacitors [23]. Furthermore, the Raman spectrum obtained demonstrates the existence of MnO_2 (Figure 3e). The band at 650.4 cm^{-1}, which is absent in the Raman spectrum of a bare CNT fiber, can be assigned to the A_{1g} mode and is indicative of a well-developed rutile-type framework [38], whereas the bands at 1325.1 cm^{-1} and

1584.2 cm^{-1} are regarded respectively as the D and G band of CNT. Characterisation by X-ray photoelectron spectroscopy (XPS) shows that the bending energy separation between the Mn $2p_{1/2}$ and Mn $2p_{2/3}$ doublet peaks is 11.8 eV, which is in agreement with the reported energy separation in MnO_2 (Figure 3f) [39]. Therefore, it can be concluded that this non-vacuum-based, scalable, and cost-effective electrochemical deposition technique has achieved successful hybrid structure formation for wet-spun, pseudocapacitive fiber electrodes. The electrochemical energy storage reaction of the hybrid CNT fiber is due to the nanoscopic surface of MnO_2, and the loading amount of MnO_2 can be well controlled by adjusting its deposition time to obtain high capacitances and high-rate capability simultaneously. Therefore, with the increase of deposition time from 10 s to 60 min, the thickness of coated MnO_2 gradually increased from around 110 nm to 9.9 μm (Figure S3). The surface of wet-spun CNT fiber can be completely covered by MnO_2 nanoflakes after 1 min of electrodeposition, which is significantly different from the reported results that indicate a required fully covered deposition time of 20 min [7]. The reason for this improvement is the much higher conductivity of single-walled CNT fiber and higher applied voltage so that the electrons transfer faster between the surface of the fiber and the electrolyte. The electrical conductivity of MCFs with different electrodeposition time was measured using a four-probe method and the linear resistances of fibers have also been calculated (Figure S4 supporting information). As expected, the electrical conductivity of MCFs decreased with increased electrodeposition time owing to the intrinsically low conductivity of MnO_2 (10^{-5}-10^{-6} S/cm) [40].

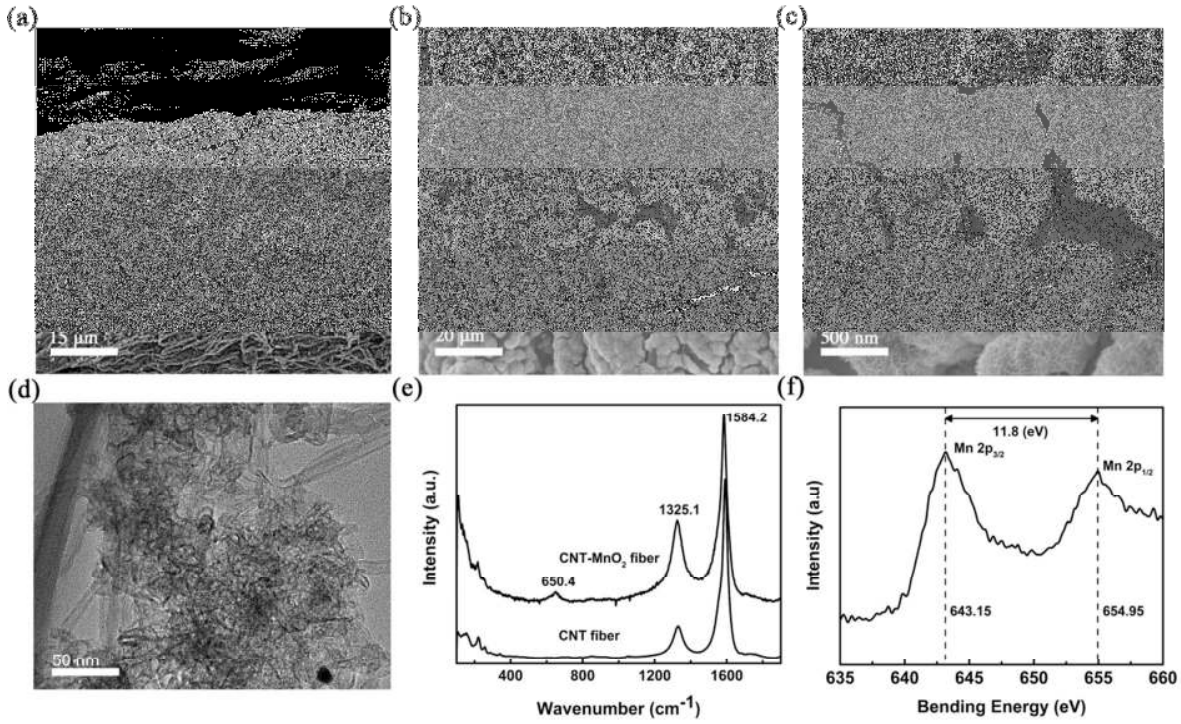

Figure 3. (a) SEM images of the surfaces of hybrid CNT fiber after mesoporous MnO_2 deposition for over 20s and (b-c) higher magnification. (d) TEM image of carbon nanotubes overlaid with highly porous MnO_2 structure. (e) Raman spectra of bare CNT fiber and MnO_2 deposited fiber, illustrating the peak of MnO_2. (f) XPS of as-grown MnO_2 nanostructure showing the bending energy of Mn 2p. The binding energy difference between the Mn 2p doublet peaks is 11.8 eV, which corresponds to that expected for MnO_2 [27].

To confirm the role that CNT fibers played in the electrodes rather than relying solely on the MnO_2 deposited on the fiber surface, we deposited MnO_2 onto a CNT fiber and a stainless steel wire (MSS), which also had a high conductivity, as comparative electrodes at the same time. Cyclic voltammograms (CV) of a bare CNT fiber, MCF and MSS are shown in Figure S5, the CV curves were measured using a three-electrode system in 1M Na_2SO_4 solution at room temperature, the scan rate was 20 mV/s. We found that CNT fiber itself has a capacitance and exhibits a rectangular shaped CV curve like MCF, however MSS showed a poor specific

capacitance. The weight of deposited MnO_2 was used to calculate the capacitance of the MSS sample while the mass of deposited MnO_2 and CNT fiber were used for the MCF sample to reflect the synergistic effect between CNT fiber and MnO_2. Consequently the stainless steel wire/MnO_2 exhibits considerably poorer capacitance compared with CNT and MCF. In addition, it was experimentally confirmed that strong adhesion of the MnO_2 nanoflakes to the porous wet-spun CNT fiber was achieved, thus high electrochemical stability could be demonstrated against repeated mechanical deformation by bending or electrochemical reaction, however, the MnO_2 on stainless steel wire can be easily wiped off after a few cycles.

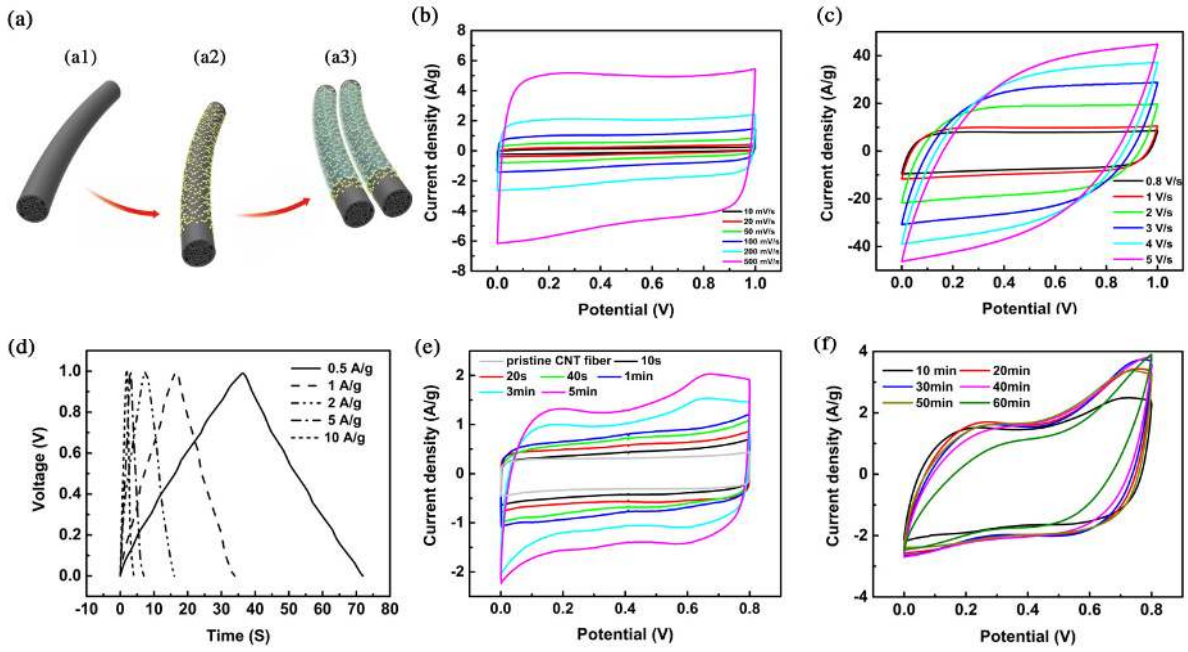

Figure 4. (a) Schematic diagram of two symmetric pseudocapacitive hybrid wet-spun CNT fiber-based supercapacitor, (a1) as-prepared CNT fiber, (a2) MnO_2 deposited onto the CNT fiber and (a3) assembled device in a parallel configuration with constant gap and coated with aqueous PVA-based gel containing LiCl. Cyclic voltammograms of a CNT fiber-based supercapacitor with scan rate (b) from 100 mV/s to 500 mV/s and (c) from 0.8 V/s to 5 V/s. (d) Galvanostatic charge-discharge curves of the device at a current density range of 0.5 A/g to 10 A/g, (e) and (f)

CV curves of a single MnO_2 deposited fiber electrode with different deposition time from 10 s to 60 min at a scan rate of 20 mV/s.

The schematic diagram of two symmetric pseudocapcitive hybrid wet-spun CNT fiber electrodes assembled in a parallel configuration with a gap to prevent short circuit and coated with aqueous poly(vinyl alcohol) containing lithium chloride is shown in Figure 4a. To evaluate the performance of the as-prepared hybrid CNT fiber as a supercapacitor, two symmetric fiber-based supercapacitors have been prepared, including two bare wet-spun CNT fibers and hybrid CNT/MnO_2 fibers. Consistent with a typical double layer capacitive material, CNT fiber-based supercapacitor (FSC) can almost keep the rectangular CV shape even at a high scan rate of 3 V/s when the device is operated at scan rates ranging from 0.01 to 5 V/s (Figure 4b, c). In the same way, it shows a minuscule equivalent series resistance (ESR) of the CNT fiber, and the porous structure simultaneously induces rapid ion diffusion into the fiber. The galvanostatic charge-discharge (GCD) measurement of pristine CNT fiber was carried out to evaluate the specific capacitance of the device (Figure 4d) at different current densities from 0.5 to 10 A/g. The curve demonstrates an isosceles triangle and the potential of the discharge curve is linear with time, indicating a good reversibility of the electrode reaction as well as a superior EDLC capacitive behavior. From the above measurements, the existence of MnO_2 can significantly enhance the specific capacitance of CNT fiber; as evidenced by comparing the absolute area calculated from the CV curves before and after MnO_2 deposition. It was found that the specific capacitance of the MnO_2 deposited fiber-based supercapacitor is approximately 230% higher than the pristine CNT fiber device at the same current density of 0.5 A/g.

Since the active surface area of MnO_2 determines the energy storagecapacity, thin MnO_2 nanoflakes (thickness 5 μm, see Figure S3) were obtained by adjusting the deposition time to 20 min. This resulted in high capacitance and high charge/discharge rate capability [41]. It was found that the amount of MnO_2 on the fiber after 20 min deposition substantially drives down the electrical conductivity with more pseudocapacitance rather than double-layer capacitance obtained (see Figure S5 for more information) [42]. Consequently, the shapes of CV curves with different deposition times change from symmetrical to asymmetrical after depositing for more than 20 min (Figure 4e, f). The relationship between the capability of MCF and deposition time is listed in Figure S6 and we find that the highest specific capacitance is obtained when the deposition time is 20 min with a value of 94.9 F/g at a scan rate of 20 mV/s. The mechanism is based on the surface adsorption of electrolyte cations (C+) on MnO_2:

$$(MnO_2)_{surface} + C^+ + e^- \Leftrightarrow (MnO_2{}^- C^+)_{surface} \quad (1)$$

where $C^+ = Na^+, K^+, Li^+$, and involved a redox reaction between the III and IV oxidation states of Mn [43]. Therefore we have introduced a new structural strategy (wet-spinning of composite materials) for electrode design in order to enhance the electrical conductivity and facilitate the full utilization of MnO_2 by incorporating CNT as an effective electron pathway [23, 44].

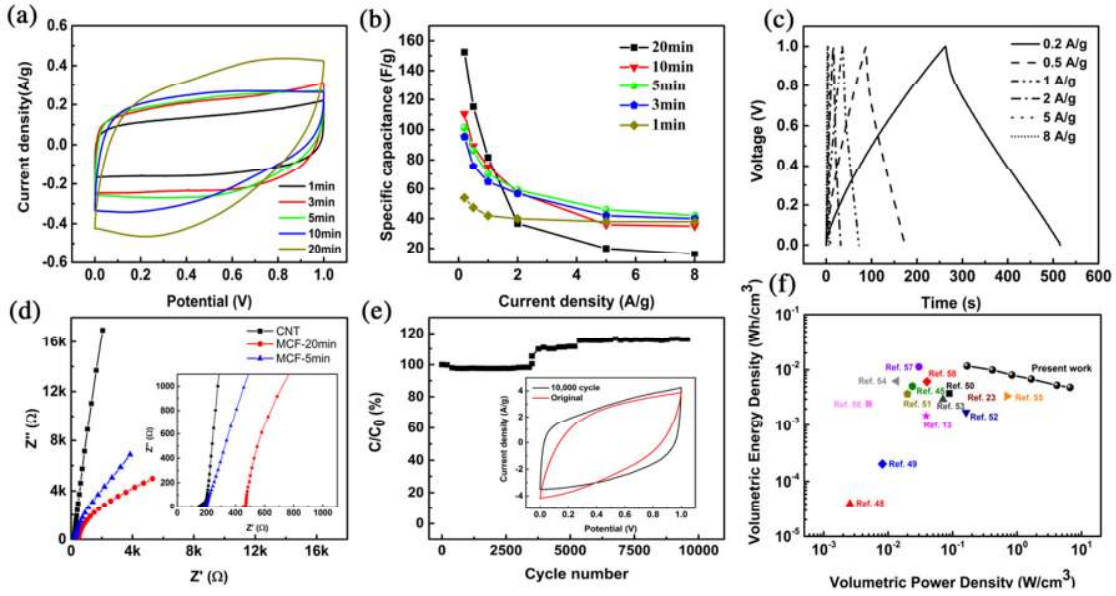

Figure 5. (a) Cyclic voltammograms of MCF supercapacitors with different deposition times ranging from 1min to 20 min at a scan rate of 5 mV/s. (b) Specific capacitances of the devices and (c) Galvanostatic charge discharge curves of the device with 5 min deposited MnO_2 layer at a current density range of 0.2 A/g to 8 A/g. (d) Nyquist plots of supercapacitors with different electrode systems. (e) Capacity retention of the 5 min device with 10,000 cycles (the inset is the CV curves of selected device before and after cycling measurement at a scan rate of 100 mV/s). (f) Plots of energy density vs power density for our fiber-based supercapacitor and other reported supercapacitors.

To demonstrate the application of the developed hybrid fiber as a supercapacitor, we assembled the MCF into highly flexible and solid-state supercapacitors by using the LiCl/PVA as both electrolyte and separator. Figure 5a shows cyclic voltammograms of the fiber-based supercapacitors with different MnO_2 deposition times ranging from 1 min to 20 min at a scan rate of 5 mV/s. The CV curves show a significant shape change with increasing deposition time and evidence of redox reactions of MnO_2. Similarly, specific capacitances calculations from galvanostatic charge-discharge measurements were also carried out to corroborate the lower rate capability that pseudocapacitive materials exhibit (Figure 5b). The highest specific capacitance

was afforded by the 20 min deposited MCF supercapacitor; with a value of 152.4 F/g at a current density of 0.2 A/g, which matches the trend that one fiber expressed above. This value is much higher than those of electrodeposited fiber-based supercapacitors with the substrates of MWNT yarn, cotton yarns and rGO fiber reported previously (converting to volume capacitance of 156.9 F/cm^3, where the density of 20 min deposited MCF is about 1.03 g/cm^3 by averaging at least 5 fibers) [7, 24, 45]. It was found that the capacitance decreases to 16.0 F/g at 8 A/g. Therefore, we selected the device with the deposition time of 5 min as a more practical application for further measurements; as it afforded a high specific capacitance of 101.4 F/g at 0.2 A/g and 42.1 F/g at 8 A/g. An ultrafast charge-discharge rate and a very small voltage drop of the selected device are evident in Figure 5c. The discharge time for the MnO_2-CNT system was effectively prolonged, by about 240% compared to the CNT system at the same current density of 0.5 A/g. Figure 5d shows the Nyquist plots in the frequency range from 100 kHz to 0.01 Hz, where the straight line is nearly parallel to the imaginary axis, demonstrating a decent capacitive behavior of the device; while the pure CNT fiber-based supercapacitor reveals an almost vertical line. Meanwhile, the slope of the sample at lower frequencies with 20 min deposited MnO_2 layer is much smaller than that of the sample with 5 min MnO_2 layer, implying poorer capacitive behavior [46]. With the poor electrical conductivity of MnO_2, the restricted time for fast charging/discharging curtails the charge diffusion along the electrode, leading to a deteriorating capacitive characteristic as the current density increases. On the other hand, a higher loading of MnO_2 distinctly raises the ESR of the supercapacitor in the high frequency region.

Cycling stability plays a vital role in real applications for supercapacitors. As shown in Figure 5e, cycling measurements were carried out using a current density of 1 A/g. There is almost no obvious drop of the specific capacitance after 10,000 cycles, but showing a 16%

increase after 3,500 cycles, which points to an extraordinary long-life cycling structure of the composite electrode. The first stage of the decrease can be considered as the electrochemical action of the outer layer of MnO_2. After repetitive charge-discharge cycling, the inner MnO_2 sites and CNT nano-networks are activated resulting in much more complete intercalation and de-intercalation of electrochemical species [47]. The inset CV curve also suggests a more rectangular and higher area curve after 10,000 cycles, even at a fast scan rate of 100 mV/s. For comparison, the cycling stabilities of 3 min and 10 min deposited MCF supercapacitors were tested respectively. Interestingly, the capacitances of both supercapacitors decrease after 5,000 cycles and the 10 min one shows a larger reduction (Figure S7). Differing from the aqueous electrolyte, the ions inside a PVA-based solid electrolyte transfer comparatively slower, suggesting a difficulty to intercalate a thick layer of MnO_2. It can be explained that the 3 min MCF SC has a thinner layer of MnO_2, leading to a full utilization of the electrode, while the thicker one only involved active materials partially in the charge-discharge process that hardly penetrating the deposited MnO_2 layer. The Ragone chart shows the energy density with respect to the average power density of the as-fabricated all solid-state supercapacitors (Figure 5f). The highest values of energy and average power densities of the 5 min MCF supercapacitor are 11.7 mWh/cm^3 and 167.7 mW/cm^3, respectively (the average density is 0.83 g/cm^3). Notably, the developed hybrid CNT fiber-based supercapacitor exhibited remarkably higher power and energy densities than reported wire-shaped supercapacitors consisting of carbon fibers coated with MnO_2/ZnO [48], MnO_2/carbon fibers [49, 50], rGO/MWNT-MoS_2/rGO/MWNT [13], GCF/N2-GCF/MnO_2 [51], MnO2/RGO/CF-GH/CW [52] and CNT/MnO_2-CNT/PPy [53] fiber-based asymmetric supercapacitor, MnO_2/MWNT fiber [23] and MnO_2/rGO fiber [45], SWNT/rGO fibers [54, 55], rGO/Activated carbon fibers [56], MnO_2/PEDOT:PSS/CNT fibers

[57], PPy/MnO_2/Carbon fibers [58], as shown in Figure 5f. The basis of wet-spun CNT fiber makes a contribution to the high power density than other carbon-based fibers and the introduction of high-performance psudocapacitance material of MnO_2 then significantly increases the energy density of our fiber-based supercapacitor. We believe that such power and energy densities mainly originate from both the CNT fiber's unique morphologies and good adhesion of MnO_2 to the collector in our case. It was experimentally demonstrated that high electrochemical stability was afforded against repeated mechanical deformation (bending). Figure S8 shows the CV performances at a scan rate of 50 mV/s as a function of different bending angles. As can be seen, the CV shapes are very stable up to 180° bending, which confirmed that the as-prepared hybrid CNT fiber-based supercapacitor with solid-state electrolyte is highly flexible and feasible to be applied for wearable electronics.

The demonstration of fiber-based supercapacitors connected in parallel powering a light-emitting diode (LED) is shown in Figure 6 a-b. The CV curves in Figure 6c show that the output current (five in parallel assembly) increased by almost five-fold with the same potential window from 0 to 1 V. This shows the potential that the fiber-based supercapacitors have for applications in wearable devices and electronic textiles.

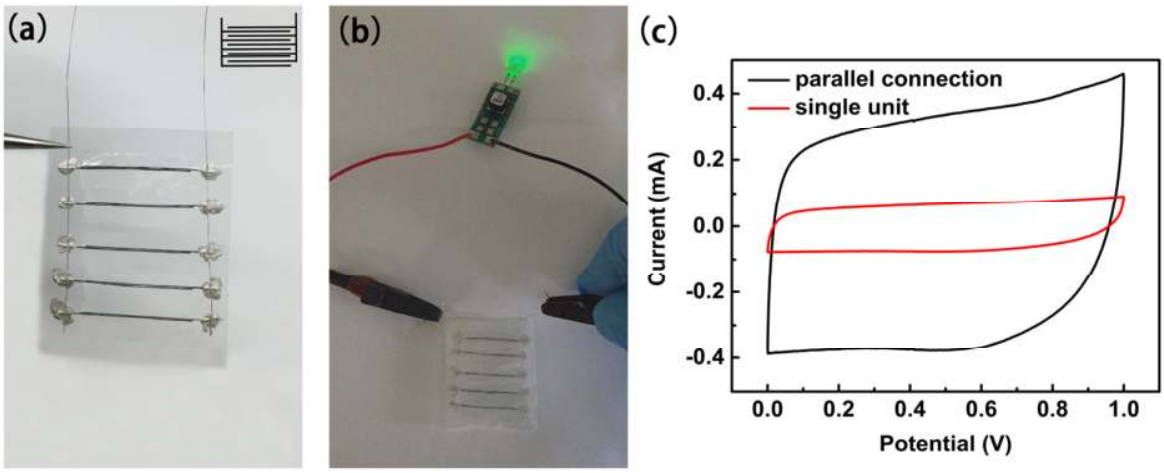

Figure 6. The electrochemical performance of the fiber-based supercapacitors in parallel. (a) Five units in parallel (inset shows the configuration of those supercapacitors in parallel). (b) Potential application of the paralleled supercapacitor, which can power a light-emitting diode independently. (c) Cyclic voltammograms of the unit and parallel circuit.

Conclusion

Highly flexible hybrid wet-spun carbon nanotube/ manganese dioxide nanocomposite fibers were fabricated. The inner nano-network structure of CNT fiber and the mesoporous flower-like MnO_2 nanoflakes facilitated the ion transport resulting in enhanced electrochemical properties. The assembled solid-state, fiber-based symmetric supercapacitor demonstrated high specific capacitance (over 152 F/g), good rate, and high cycling retention ability (over 10,000 cycles) at fast charge/discharge rate, and significantly practical energy and power densities. Our strategy provides a new direction for manufacturing of wet-spun CNT nanocomposite fibers supercapacitors. Prepared hybrid CNT fibers can benefit such applications as high-performance supercapacitors, batteries, smart textile and wearable electronics.

Acknowledgements

This work has been supported by the Australian Research Council under the Discovery Early Career Researcher Award (J. Foroughi, DE12010517), the Australian Research Council Centre of Excellence Scheme (Project Number CE 140100012) and the Australian Laureate Fellowship scheme (FL110100196). Zan Lu acknowledges the support of CSC scholarships from the Ministry of Education of P. R. China. The authors acknowledge AIIM (Australian Institute for Innovative Materials) funding (AIIM for Gold), the use of facilities within the UOW Electron Microscopy Centre, and the Australian National Nanofabrication Facility- Materials Node (ANFF).

References

[1] M.R. Lee, R.D. Eckert, K. Forberich, G. Dennler, C.J. Brabec, R.A. Gaudiana, Science 324 (2009) 232-235.

[2] S. Zhang, C. Ji, Z. Bian, P. Yu, L. Zhang, D. Liu, E. Shi, Y. Shang, H. Peng, Q. Cheng, D. Wang, C. Huang, A. Cao, ACS Nano 6 (2012) 7191-7198.

[3] D. Liu, M. Zhao, Y. Li, Z. Bian, L. Zhang, Y. Shang, X. Xia, S. Zhang, D. Yun, Z. Liu, A. Cao, C. Huang, ACS Nano 6 (2012) 11027-11034.

[4] F. Gao, L. Viry, M. Maugey, P. Poulin, N. Mano, Nat. Commun. 1 (2010) 2.

[5] M. Lee, C.Y. Chen, S. Wang, S.N. Cha, Y.J. Park, J.M. Kim, L.J. Chou, Z.L. Wang, Adv. Mater. 24 (2012) 1759-1764.

[6] A. Yadav, K. Pipe, M. Shtein, J. Power Sources 175 (2008) 909-913.

[7] N. Liu, W. Ma, J. Tao, X. Zhang, J. Su, L. Li, C. Yang, Y. Gao, D. Golberg, Y. Bando, Adv. Mater. 25 (2013) 4925-4931.

[8] V.T. Le, H. Kim, A. Ghosh, J. Kim, J. Chang, Q.A. Vu, D.T. Pham, J.-H. Lee, S.-W. Kim, Y.H. Lee, ACS nano 7 (2013) 5940-5947.

[9] G. Qu, J. Cheng, X. Li, D. Yuan, P. Chen, X. Chen, B. Wang, H. Peng, Adv. Mater. 28 (2016) 3646-3652.

[10] D. Yu, K. Goh, Q. Zhang, L. Wei, H. Wang, W. Jiang, Y. Chen, Adv. Mater. 26 (2014) 6790-6797.

[11] C.S. Haines, M.D. Lima, N. Li, G.M. Spinks, J. Foroughi, J.D. Madden, S.H. Kim, S. Fang, M. Jung de Andrade, F. Goktepe, O. Goktepe, S.M. Mirvakili, S. Naficy, X. Lepro, J. Oh, M.E. Kozlov, S.J. Kim, X. Xu, B.J. Swedlove, G.G. Wallace, R.H. Baughman, Science 343 (2014) 868-872.

[12] J. Foroughi, G.M. Spinks, G.G. Wallace, J. Oh, M.E. Kozlov, S. Fang, T. Mirfakhrai, J.D. Madden, M.K. Shin, S.J. Kim, R.H. Baughman, Science 334 (2011) 494-497.

[13] G. Sun, X. Zhang, R. Lin, J. Yang, H. Zhang, P. Chen, Angew. Chem. 127 (2015) 4734-4739.

[14] J. Foroughi, G.M. Spinks, S. Aziz, A. Mirabedini, A. Jeiranikhameneh, G.G. Wallace, M.E. Kozlov, R.H. Baughman, ACS nano 10 (2016) 9129-9135.

[15] P. Jarosz, C. Schauerman, J. Alvarenga, B. Moses, T. Mastrangelo, R. Raffaelle, R. Ridgley, B. Landi, Nanoscale 3 (2011) 4542-4553.

[16] P.R. Jarosz, A. Shaukat, C.M. Schauerman, C.D. Cress, P.E. Kladitis, R.D. Ridgley, B.J. Landi, ACS Appl. Mater. Interfaces 4 (2012) 1103-1109.

[17] D. Pech, M. Brunet, H. Durou, P. Huang, V. Mochalin, Y. Gogotsi, P.L. Taberna, P. Simon, Nat. Nanotech. 5 (2010) 651-654.

[18] M.F. El-Kady, V. Strong, S. Dubin, R.B. Kaner, Science 335 (2012) 1326-1330.

[19] P. Simon, Y. Gogotsi, Nat. Mater. 7 (2008) 845-854.

[20] J.R. Miller, P. Simon, Science 321 (2008) 651-652.

[21] F. Yao, D.T. Pham, Y.H. Lee, ChemSusChem 8 (2015) 2284-2311.

[22] K. Wang, Q. Meng, Y. Zhang, Z. Wei, M. Miao, Adv. Mater. 25 (2013) 1494-1498.

[23] C. Choi, J.A. Lee, A.Y. Choi, Y.T. Kim, X. Lepró, M.D. Lima, R.H. Baughman, S.J. Kim, Adv. Mater. 26 (2014) 2059-2065.

[24] Z. Cai, L. Li, J. Ren, L. Qiu, H. Lin, H. Peng, J. Mater. Chem. A 1 (2013) 258-261.

[25] X. Chen, H. Lin, J. Deng, Y. Zhang, X. Sun, P. Chen, X. Fang, Z. Zhang, G. Guan, H. Peng, Adv. Mater. 26 (2014) 8126-8132.

[26] S. Chen, W. Ma, Y. Cheng, Z. Weng, B. Sun, L. Wang, W. Chen, F. Li, M. Zhu, H.-M. Cheng, Nano Energy 15 (2015) 642-653.

[27] C. Choi, H.J. Sim, G.M. Spinks, X. Lepró, R.H. Baughman, S.J. Kim, Adv. Eng. Mater. (2016) 1502119.

[28] C. Choi, S.H. Kim, H.J. Sim, J.A. Lee, A.Y. Choi, Y.T. Kim, X. Lepró, G.M. Spinks, R.H. Baughman, S.J. Kim, Sci. Rep. 5 (2015).

[29] N. Behabtu, C.C. Young, D.E. Tsentalovich, O. Kleinerman, X. Wang, A.W. Ma, E.A. Bengio, R.F. ter Waarbeek, J.J. de Jong, R.E. Hoogerwerf, S.B. Fairchild, J.B. Ferguson, B. Maruyama, J. Kono, Y. Talmon, Y. Cohen, M.J. Otto, M. Pasquali, Science 339 (2013) 182-186.

[30] B. Zheng, T. Huang, L. Kou, X. Zhao, K. Gopalsamy, C. Gao, J. Mater. Chem. A 2 (2014) 9736-9743.

[31] V.A. Davis, A.N.G. Parra-Vasquez, M.J. Green, P.K. Rai, N. Behabtu, V. Prieto, R.D. Booker, J. Schmidt, E. Kesselman, W. Zhou, Nat. Nanotech. 4 (2009) 830-834.

[32] A.R. Bucossi, C.D. Cress, C.M. Schauerman, J.E. Rossi, I. Puchades, B.J. Landi, ACS Appl. Mater. Interfaces 7 (2015) 27299-27305.

[33] S. Zhang, K.K. Koziol, I.A. Kinloch, A.H. Windle, Small 4 (2008) 1217-1222.

[34] L.M. Ericson, H. Fan, H. Peng, V.A. Davis, W. Zhou, J. Sulpizio, Y. Wang, R. Booker, J. Vavro, C. Guthy, A.N. Parra-Vasquez, M.J. Kim, S. Ramesh, R.K. Saini, C. Kittrell, G. Lavin, H. Schmidt, W.W. Adams, W.E. Billups, M. Pasquali, W.F. Hwang, R.H. Hauge, J.E. Fischer, R.E. Smalley, Science 305 (2004) 1447-1450.

[35] M. Zhang, K.R. Atkinson, R.H. Baughman, Science 306 (2004) 1358-1361.

[36] C. Jiang, A. Saha, C.C. Young, D.P. Hashim, C.E. Ramirez, P.M. Ajayan, M. Pasquali, A.A. Marti, ACS Nano 8 (2014) 9107-9112.

[37] X. Lang, A. Hirata, T. Fujita, M. Chen, Nat. Nanotech. 6 (2011) 232-236.

[38] T. Gao, H. Fjellvag, P. Norby, Anal. Chim. Acta 648 (2009) 235-239.

[39] S.W. Lee, J. Kim, S. Chen, P.T. Hammond, Y. Shao-Horn, ACS Nano 4 (2010) 3889-3896.

[40] C. Xu, F. Kang, B. Li, H. Du, J. Mater. Res. 25 (2010) 1421-1432.

[41] M. Toupin, T. Brousse, D. Bélanger, Chem. Mater. 16 (2004) 3184-3190.

[42] T. Brousse, D. Bélanger, J.W. Long, J. Electrochem. Soc. 162 (2015) A5185-A5189.

[43] H.Y. Lee, J.B. Goodenough, J. Solid State Chem. 144 (1999) 220-223.

[44] Z. Li, Y. Mi, X. Liu, S. Liu, S. Yang, J. Wang, J. Mat. Chem. 21 (2011) 14706-14711.

[45] W. Ma, S. Chen, S. Yang, W. Chen, Y. Cheng, Y. Guo, S. Peng, S. Ramakrishna, M. Zhu, J. Power Sources 306 (2016) 481-488.

[46] G. Yu, L. Hu, N. Liu, H. Wang, M. Vosgueritchian, Y. Yang, Y. Cui, Z. Bao, Nano Lett. 11 (2011) 4438-4442.

[47] X. Lu, D. Zheng, T. Zhai, Z. Liu, Y. Huang, S. Xie, Y. Tong, Energ. Environ. Sci. 4 (2011) 2915-2921.

[48] P. Yang, X. Xiao, Y. Li, Y. Ding, P. Qiang, X. Tan, W. Mai, Z. Lin, W. Wu, T. Li, H. Jin, P. Liu, J. Zhou, C.P. Wong, Z.L. Wang, ACS Nano 7 (2013) 2617-2626.

[49] X. Xiao, T. Li, P. Yang, Y. Gao, H. Jin, W. Ni, W. Zhan, X. Zhang, Y. Cao, J. Zhong, L. Gong, W.C. Yen, W. Mai, J. Chen, K. Huo, Y.L. Chueh, Z.L. Wang, J. Zhou, ACS Nano 6 (2012) 9200-9206.

[50] J. Zhang, X. Zhao, Z. Huang, T. Xu, Q. Zhang, Carbon 107 (2016) 844-851.

[51] D. Yu, K. Goh, Q. Zhang, L. Wei, H. Wang, W. Jiang, Y. Chen, Adv. Mater. 26 (2014) 6790-6797.

[52] Z. Zhang, F. Xiao, S. Wang, J. Mater. Chem. A 3 (2015) 11215-11223.

[53] J. Yu, W. Lu, J.P. Smith, K.S. Booksh, L. Meng, Y. Huang, Q. Li, J.H. Byun, Y. Oh, Y. Yan, Adv. Energ. Mater. (2016).

[54] D. Yu, K. Goh, H. Wang, L. Wei, W. Jiang, Q. Zhang, L. Dai, Y. Chen, Nat. Nanotech. 9 (2014) 555-562.

[55] Y. Ma, P. Li, J.W. Sedloff, X. Zhang, H. Zhang, J. Liu, ACS nano 9 (2015) 1352-1359.

[56] W. Ma, S. Chen, S. Yang, W. Chen, W. Weng, M. Zhu, ACS Appl. Mater. Interfaces 8 (2016) 14622-14627.

[57] X.-L. Cheng, J. Zhang, J. Ren, N. Liu, P. Chen, Y. Zhang, J. Deng, Y.-G. Wang, H. Peng, J. Phys. Chem. C 120 (2016) 9685-9691.

[58] J. Tao, N. Liu, W. Ma, L. Ding, L. Li, J. Su, Y. Gao, Sci. Rep. 3 (2013) 2286.